Chapter 6

Light-Emitting Diodes based on alternating PPV copolymers and oligo(*p*-phenylene vinylene)s†

Abstract

In this chapter the performance of several novel alternating PPV copolymers and 5-ring oligo(p-phenylene vinylene)s as active layer in LEDs are presented. The colour of emission of the copolymers and oligomers is varied by means of different substituents (cyanogroups, alkyl/alkoxy side-chains), attached to the conjugated backbone, which alter the electronic structure of the molecules. Electroluminescence in the blue, green and orange wavelength region was achieved in single-layer devices with air-stable Al cathodes. The external electroluminescence efficiencies of all single-layer devices were found to be in the range of 0.01 to 0.03 % photons/electron, values comparable to those reported for fully conjugated PPVs. The influence of the thin-film morphology on LED performance has been investigated for the 5-ring oligomers. For Ooct-OPV5 a more than tenfold increase in efficiency was observed for devices consisting of an annealed active layer, which has been attributed to enhanced electron transport upon annealing.

Device optimization by means of additional charge-transport layers has been applied to enhance the electroluminescence efficiency. A novel polymer with oxadiazole-based side-chains has been used successfully as an electron-transport/hole-blocking layer. In combination with a PPV copolymer as the emissive layer, external EL efficiencies up to 0.1 % were obtained. The best-performing double-layer LEDs were based on the cyano-substituted copolymers and oligomers as the electron-transport/emissive layer. In this case, external electroluminescence efficiencies up to 0.4 % are reached.

---

† H.J. Brouwer, A. Hilberer, V.V. Krasnikov, M.P.L. Werts, G. Hadziioannou, *Synth. Met.*, **84**, 881 (1997)

6.1 Introduction

The most widely used semiconducting polymers for application in light-emitting diodes are poly(*p*-phenylene vinylene) (PPV) and its derivatives, which have the highest luminescence efficiencies of all conjugated polymers. Their excellent emissive properties already have been demonstrated in chapter 3 in 4, where photopumped lasing of PPV polymers in solution and solid state has been described. After the introduction of Light-Emitting Diodes (LEDs) based on PPV in 1990 by Friend et al. [1], a lot of research in the field of semiconducting polymers has been directed towards the development of new efficient polymeric emitters (for a recent review see [2,3]). A whole range of polymeric LEDs, emitting over the whole visible wavelength region from blue to red, has been reported [4,5]. Furthermore, the LED performance was greatly improved by means of additional charge-transport layers, which effectively balance the injection and transport of charges and move the e-h recombination zone away from the metal cathode [6]. Double-layer LEDs with high peak brightness and internal electroluminescence efficiencies up to 4 % [7] have been reported. Nevertheless, no commercial polymer LEDs has been manufactured yet. The long-term device stability and device efficiencies of polymer LEDs are rapidly increasing, but improvements are still desired, especially for polymers emitting in the blue wavelength region.

In conjugated polymers and oligomers, the overlap of π-orbitals provides a continuous system of electron density along the molecular backbone. The extent of this overlap (the so-called conjugation length) determines the HOMO-LUMO energy gap, which is, in general, found to be within the visible wavelength region. In conjugated homopolymers, the actual conjugation length is an average value determined principally by random conformational or chemical defects in the polymer backbone and is difficult to control. Our approach to controlling the conjugation length (described in chapter 1) and making the link between the luminescence properties of oligomers and those of polymers, is through alternating copolymers containing well-defined conjugated sequences with non-conjugated spacer units. This approach is particularly suitable for the design of blue-light emitters, which have a large HOMO-LUMO gap. This demands a high degree of control over the conjugation length. Furthermore, this approach can enhance the photo- and electroluminescence efficiency through confinement of the excitons to the conjugated blocks, which hinders the migration to quenching sites [8]. Braun *et al.* [9] showed that the PL efficiency increased with increasing fraction of the non-conjugated blocks in the backbone. Blue-light emitting devices with external efficiencies up to 0.7 % [10] were reported by our group with alternating SiPPV copolymers made according this concept.

PPV oligomers gained considerable interest, both as model compounds [11] and for application as active layer in LEDs [12,13]. They are highly fluorescent, have

a well-defined chemical structure and conjugation length and the ability to crystallize into well-ordered molecular crystals, which allows structural information to be obtained. Furthermore, they can be processed by vacuum deposition from the vapour phase into high-purity thin films. The morphology of the thin films can be controlled by means of adjustment of the substrate temperature during evaporation, or like in our case an annealling treatment after deposition. At low temperature the molecules stick where they collide, but at a substrate temperature close to the melting point of the oligomer, the molecules have sufficient thermal energy to diffuse and to minimize their structural energy, resulting in a more ordered packing. For example, in the case of α-sexithiophene, this led to improved transport properties [14]. Furthermore, the control of molecular order allows the systematic investigation of the influence of thin-film morphology on LED performance.

In this chapter we evaluate the electrical and optical characteristics of light-emitting diodes based on alternating PPV copolymers and 5-ring oligo(*p*-phenylene vinylene)s. The colour of emission of the copolymers and oligomers is varied by means of different substituents (cyano, alkoxy), attached to the conjugated backbone, which alter the electronic structure of the molecules. Electroluminescence was achieved in the blue, green and orange wavelength region with single-layer devices consisting of transparent indium-tin-oxide anodes and air-stable Al cathodes. The efficiencies of the single-layer copolymer/oligomer LEDs are comparable to those reported for fully conjugated PPVs. Fowler-Nordheim tunnelling theory was used to analyse the current-voltage characteristics in order to determine the barriers for hole-injection in the single-layer devices. In combination with cyclic voltammetry and optical absorption measurements it was possible to estimate energy diagrams for all copolymers and oligomers, which could be used to describe the results obtained in a qualitative way. Furthermore, the influence of the thin-film morphology on LED performance has been investigated for the octyloxy-substituted oligo(*p*-phenylene vinylene).

Device optimization by means of additional charge-transport layers was applied to enhance the electroluminescence efficiency. A novel polymer with oxadiazole-based side-chains was used successfully as an electron-transport/hole-blocking layer, in a double-layer configuration with an orange-light-emitting PPV copolymer as the emissive layer. Also single-layer devices based on blends of the transport polymer and the PPV copolymer were studied.

The best-performing copolymer and oligomer double-layer devices were obtained by using an electronegative cyano-substituted PPV copolymer/oligomer as the electron-transport/emissive layer in combination with a hole-transport layer.

6.2. Experimental

Sample preparation

Polymer light-emitting diodes (PLEDs) were fabricated by spincoating the copolymers from filtered (0.2 μm-filters) chloroform solutions (3% w/w) onto 20 mm^2 ITO-covered glass slides (Merck Balzers AG, sheet resistance ≤ 200Ω/□). The ITO plates were ultrasonically cleaned in a series of nonpolar and polar solvents (*p*-xylene/2-propanol/ethanol) and rinsed in de-ionized water prior to use. By varying the rotation speed in the range of 700-2500 rpm, film thicknesses of 50-175 nm were obtained. The polymer films were dried for one hour at 40°C in a vacuum oven. Oligomer light-emitting diodes (OLEDs) were prepared by slow evaporation (pressure ≈10^{-6} mbar, evaporation rate 2-4 Å/s) of the compounds from a molybdenum boat just above their melting point, with the ITO plates positioned about 10 cm above the boat. The home-built evaporator was equipped with two separate sources, which enabled us to prepare double-layer devices in one run. Al or Au top electrodes (area: 1 × 9 mm^2) were deposited by evaporation (pressure < 2×10^{-6} mbar, evaporation rate < 5 Å/s, thickness ≈ 80 nm) through a shadow mask. The active area of the device 1 × 8 mm^2 is defined by the overlap of the ITO and the top metal electrode. Atomic Force Microscopy was used to monitor the quality of the copolymer and oligomer films. A Dektak 3030ST surface profiler was used to determine the layer thickness.

LED characterization

Photo- and electroluminescence spectra of the thin-film devices were recorded on a SLM-Aminco SPF500C spectrofluorometer or Perkin-Elmer LS-50B. Absorbance spectra of the thin films were measured on a SLM-Aminco 3000 Array spectrophotometer.

Current-voltage (I-V) and luminance-voltage (L-V) measurements were performed in a dry-nitrogen atmosphere glove box to avoid exposure to ambient oxygen and water. I-V-measurements were taken with a Keithley 236 SMU operated in pulsed mode (low duty cycle, t_{on}= 100 ms and t_{off}= 500 ms) to minimize heating effects. The external quantum efficiencies (number of emitted photons per injected electron) of the devices were determined by measuring the light output of the diodes vs. current with a calibrated photodiode mounted on an integrated sphere (LabSphere). A photon counter (Stanford Research SR400) was used to measure the photodiode output.

Cyclic voltammetry

Cyclic voltammetry was used to determine the oxidation potentials of the copolymers. The cyclic voltammetry measurements were performed on a Parc EG&G galvanometer using platinum working and counter electrodes and silver as the reference electrode in dichloromethane with tetrabutylammonium hexafluorophosphate as the electrolyte. The cylcovoltammograms were calibrated towards the normal hydrogen electrode (NHE) using the ferrocene/ferrocenium-ion couple as an internal standard [15,16].

Electroabsorption measurements

It is known that the work function of ITO is a poorly defined quantity, and that its value varies significantly (4.5–5.3 eV) [17,18] depending on the fabrication conditions and supplier. The built-in electric field in our metal/polymer(oligomer)/ITO diodes was determined via electroabsorption measurements [19], in order to obtain the work function of our ITO electrodes (Balzer A.G. Austria).

The electroabsorption response is proportional to the imaginary part of the third order susceptibility $\mathrm{Im}\chi^{(3)}(h\upsilon)$ and the square of the electric field.

$$\Delta\alpha(h\upsilon) \propto -\frac{\Delta T}{T}(h\upsilon) \propto \mathrm{Im}\,\chi^{(3)}(h\upsilon)\,E^2 \tag{6.1}$$

where α is the absorption coefficient, $h\upsilon$ is the photon energy, T the transmission and E the electric field. The electroabsorption response to an applied AC bias is:

$$E = E_o + E_{AC}\cos(\Omega t), \quad \Omega \cong 1kHz,$$

$$-\frac{\Delta T}{T}(h\upsilon) \propto \mathrm{Im}\,\chi^{(3)}(h\upsilon)\{E_{AC}^2[1+\cos(2\Omega t)]/2 + 2E_{AC}E_o\cos(\Omega t) + E_o^2\} \tag{6.2}$$

where E_0 is the static electric field and E_{AC} is the amplitude of the AC electric field. In the presence of a static electric field the, electroabsorption is modulated at both the fundamental and the second harmonic frequency of the applied AC voltage. The built-in electric field is measured by applying an external DC bias and finding the external potential at which the electroabsorption signal at the fundamental frequency vanishes. The built-in electric field, in a diode with a constant electric field throughout the bulk, will be equal to the difference in work function of the metal electrodes, if the work function of the metals lies within the HOMO-LUMO gap of the polymer/oligomer.

For these experiments single-layer diodes were prepared following the procedure described in the *sample preparation* section. The oligomer Ooct-OPV5 was used as active layer. Electrical measurements on several Al/Ooct-OPV5/ITO diodes with different Ooct-OPV5 layer thickness showed that the I-V-dependence scaled with the Ooct-OPV5 layer thickness (see section 6.3.2), which indicated that there is a constant electric field throughout the bulk. In figure 6.1 the electroabsorption response at λ = 510 nm is shown for 200 nm thick Ooct-OPV5 films sandwiched between Al/ITO, Au/ITO and Al/Au electrodes. The Al/Ooct-OPV5/Au device was prepared by succesive evaporation of the oligomer and Al counter electrodes onto a 40 nm thick semi-transparent Au layer on glass. The DC bias was referenced to the high work function contacts (ITO or Au). The DC bias of 1.0 Volts required to null the electroabsorption signal in the Al/Au diode corresponded closely to the difference in work function between the two metals (ϕ_{Al} = 4.2-4.3 eV and ϕ_{Au} = 5.1-5.2 eV) [20].

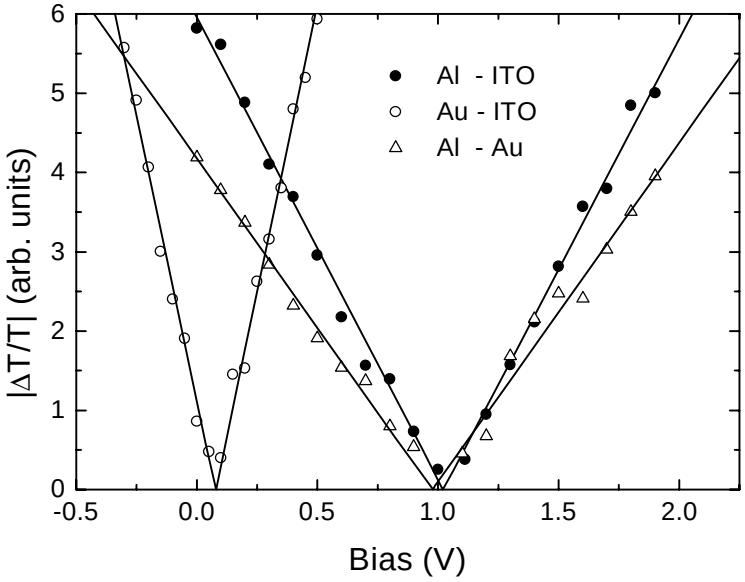

Figure 6.1 *Electroabsorption response at λ=510 nm for 200 nm thick Ooct-OPV5 films sandwiched between Al/ITO, Au/ITO and Al/Au electrodes.*

The DC biases to null the electroabsorption signal in the Al/ITO and Au/ITO devices were 1.0 and 0.1 Volts, respectively. From these measurements we determined a work function of ϕ_{ITO} = 5.2±0.1 eV for our ITO electrodes. The reproducibility of the electroabsorption measurements was good, and the same values for the ITO work

function were obtained from measurements with single-layer diodes made from the PPV based copolymers.

6.3 Results and discussion

6.3.1 Alternating PPV copolymers

A series of three alternating PPV copolymers containing substituted distyrylbenzene units as the light-emitting chromophores were used as active layer in LEDs. The chemical structures of the copolymers are depicted in figure 6.2. The substitution pattern (octyl/octyloxy side-chains and cyano groups on the vinylene linkages) in the copolymers was varied in order to tune the wavelength of emission. In such a way light emission from the blue to orange/red wavelength region was established. The synthesis and full characterization of the PPV copolymers are described in the references [21,22].

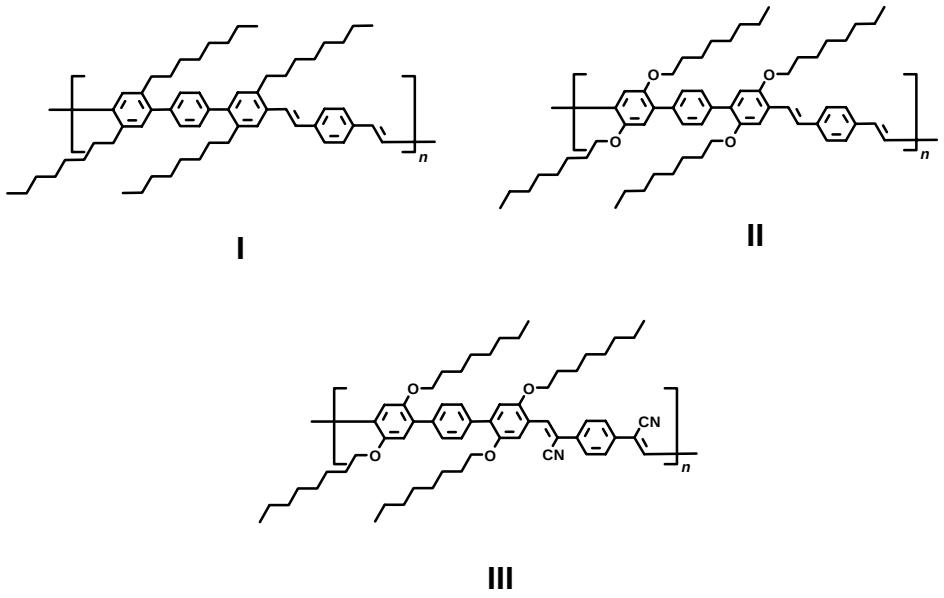

Figure 6.2 *Chemical structure of the copolymers.*

The molar masses and the solid-state optical properties are summarized in table 6.1 (see also chapter two for more detail). The copolymers have a well-defined conjugated backbone consisting of regularly alternating terphenylene and *p*-phenylenebisvinylene blocks. The desired control of conjugation length was achieved through steric interactions between the side-chains and the rings within the terphenyl part of the copolymer. The octyl and octyloxy side chains in these polymers serve a

dual role: (1) interrupting the conjugation and (2) providing solubility. The middle rings in the terphenyl units are twisted out of plane, disabling the possibility of conjugation through the three consecutive phenyl rings. Thus, the conjugation of the fully unsaturated backbone is regularly interrupted, resulting in well-defined distyrylbenzene chromophores connected by non-coplanar phenylene groups. The copolymers show intense fluorescence in solution (0.4-0.9) as well as in the solid state. The films cast from copolymer **I** and **III** have photoluminescence efficiencies in the range of 30–40 %, whereas that from copolymer **II** has a substantially lower efficiency of ≈9% (see chapter 2 for more details).

Table 6.1 *Molar masses of the copolymers and absorption, emission and PL efficiency in solid state.*

Copolymer	M_w (g.mol^{-1})[a]	M_n (g.mol^{-1})[a]	$\lambda_{Abs,max}$ (nm)	$\lambda_{Flu,max}$ (nm)	Φ_{Flu}
I	5000	3000	355	445	0.4
II	39000	22000	418	485	0.09
III	7200	6500	450	592	0.4

a) Molecular weights obtained from reference [21,22]

LED devices were prepared as described in the experimental section. Analysis with Atomic Force Microscopy showed that the film surfaces were homogeneous and pinhole-free, with a surface roughness of a few percent of the total layer thickness. The electroluminescence spectra obtained from Al/copolymer/ITO devices are shown in figure 6.3. Copolymer **I,** in which the chromophore is an alkyl-substituted distyrylbenzene unit, emits in the blue (445 nm). The change of the type of side chains from alkyl to alkoxy (copolymer **II**) shifts the emission wavelength to the green (485 nm), due to the increased electron density of the π-system induced by the electron-donating alkoxy group. Alkoxy side chains in combination with cyano substituents (copolymer **III**) results in a red shift to the orange part of the spectrum (592 nm). It has been demonstrated that cyano groups on the vinylene linkage lower both the HOMO and LUMO level, but that the LUMO level is stabilized more, resulting in a red shift [7,23]. The HOMO-LUMO gaps for the copolymers **I** to **III** determined by the onset of absorption are 3.0, 2.6 and 2.3 eV, respectively.

All electroluminescence spectra of the copolymers coincided with the solid-state photoluminescence spectra. The photoluminescence spectrum of copolymer **III** is shown in figure 6.3 as an example. This implies that the excited states (created by charge injection) responsible for light emission in a PLED, are the same as those produced by photoexcitation.

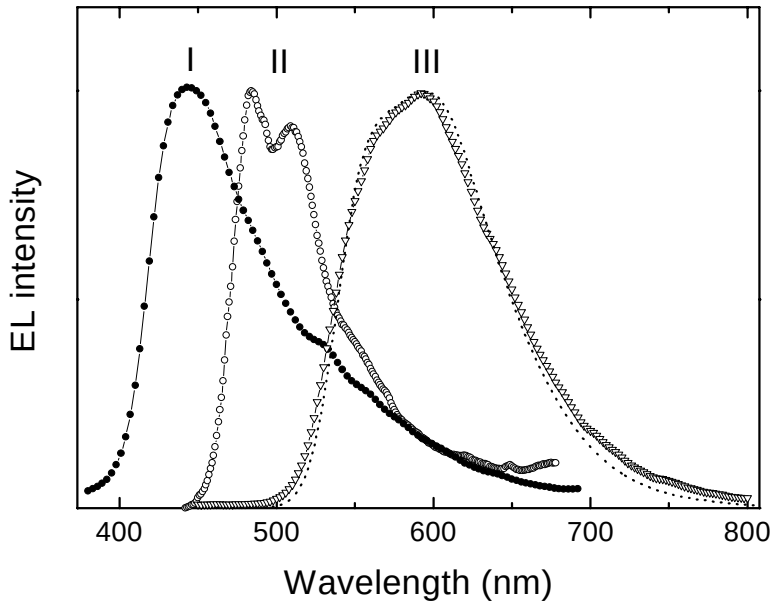

Figure 6.3 *Electroluminescence spectra of the copolymers (solid lines + symbols) and photoluminescence spectrum of copolymer **III** (dotted line).*

In figure 6.4 the current density and luminance as a function of drive voltage in forward bias are shown for a single-layer ITO/copolymer **I**/Al device with a layer thickness of 80 nm (in table 6.2 the electrical characteristics and EL efficiencies of all single-layer devices are summarized). Forward bias is defined as the positive voltage on the hole-injecting ITO contact. Electron-injecting Al contacts were chosen for reasons of stability but have the disadvantage that they limit the electron-injection rates. This is due to the relatively large difference between the molecular LUMO-levels of the polymers and the work function of Al [17,24], resulting in a high injection barrier for electrons. Additionally, there is good evidence that holes are considerably more mobile than electrons in PPV polymers due to severe trapping of electrons [25] at electron-accepting impurities, related to oxygen (molecular oxygen, carbonyl moieties, etc.). This makes these polymers preferentially hole transporters. The unbalanced electron and hole currents, due to the low injection rate and poor transport of electrons in comparison with holes, has as a consequence that there is a large (hole) loss current. In addition, since the electrons are not able to move far into the bulk due to trapping, the electron-hole recombination zone is located close to the metal cathode of the device, which has the effect of quenching the emission. Single-

layer devices therefore have low EL efficiencies. The use of the low work function metal Ca [17,26] as electron-injecting contact will result in more balanced injection, higher efficiencies and lower operating voltages but has the drawback of being highly reactive under ambient conditions.

The LEDs with copolymer **I** as active layer (80 nm) started emitting light at a turn-on voltage of 15 Volts. This corresponds to an electric field strength ($E=V/d$, d is the layer thickness) at turn-on of 1.9×10^{8} V/m (see top x-axis in figure 6.4). Turn-on voltage is defined here as the voltage at which the electroluminescence starts exceeding the background signal. It should be stated that the sensitivity for the detection of light of our set-up is low, due to the use of an integrating sphere. Only a small fraction of the photons emitted into the integrating sphere will reach the photodiode. So the turn-on voltage measured by our set-up is significantly higher as the voltage required to reach 'flat-band' conditions, which is the correct definition of the turn-on voltage [17]. The 'real' turn-on voltage is essentially independent of the layer thickness. In our case, we see a slight dependence of the turn-on voltage on the thickness of the active layer. This is due to the fact that we need to create a sufficiently large flux of photons to reach the lower detection limit of our set-up. So, the turn-on voltage obtained by our set-up also depends on the EL-efficiency of the LEDs and the quantum yield of the photodiode in the spectral region of emission.

Blue light, visible to the eye, was observed at drive voltages above 25 V. The emission was homogeneous over the whole active area at high drive voltages. The electroluminescence intensity increased linearly with drive current, and a maximum external EL-efficiency of 2.3×10^{-2} % ph/el was reached at a drive current of 8×10^{-2} A/cm^2. The current-voltage characteristics of the devices scaled with layer thickness over the range of 50–175 nm, indicating that the electric field is uniformly distributed throughout the bulk and that significant band bending is absent at both metallic interfaces. The dependence of the device current on the electric field rather than the drive voltage is considered as evidence for field-emission tunnelling of charge carriers across an interfacial barrier [17].

A change of the electron-injecting metal from Al (ϕ_{Al}= 4.3 eV) to Au (ϕ_{Au}= 5.2 eV), resulted in light emission in forward bias at a much higher turn-on voltage of 24 Volts (E = 3.0×10^{8} V/m). The external EL quantum efficiency of the diodes was $\approx3\times10^{-3}$ % ph/el. The I-V characteristics in forward and reverse bias were nearly symmetrical in the ITO/Au diodes, due to the small difference in work function between the opposite contacts. In reverse bias, light emission started at a turn-on voltage of –25 Volts. This observation supports the conclusion that field-driven electron injection determines the emissive properties of a polymer LED.

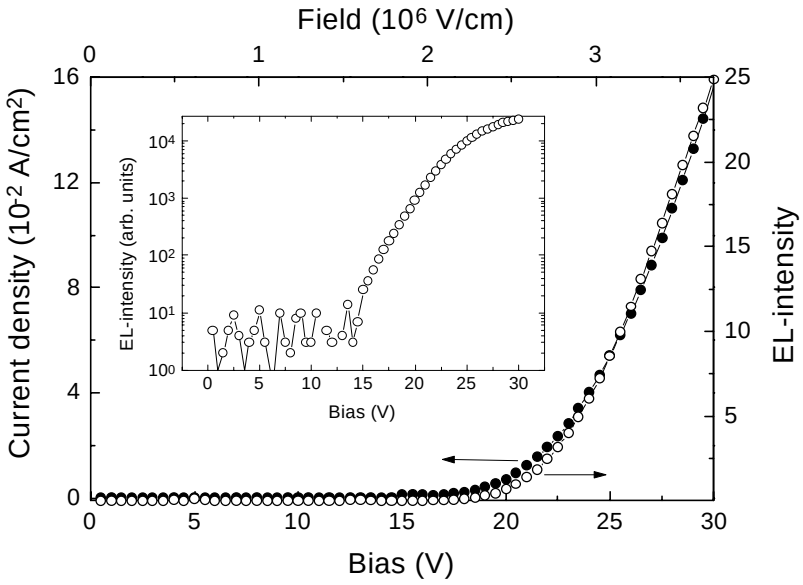

Figure 6.4 *Current density (closed circles) and luminance (open circles) of a single-layer ITO/copolymer **I**/Al device as a function of bias voltage. Layer thickness 80 nm. Inset: semilog plot of the luminance as a function of bias voltage.*

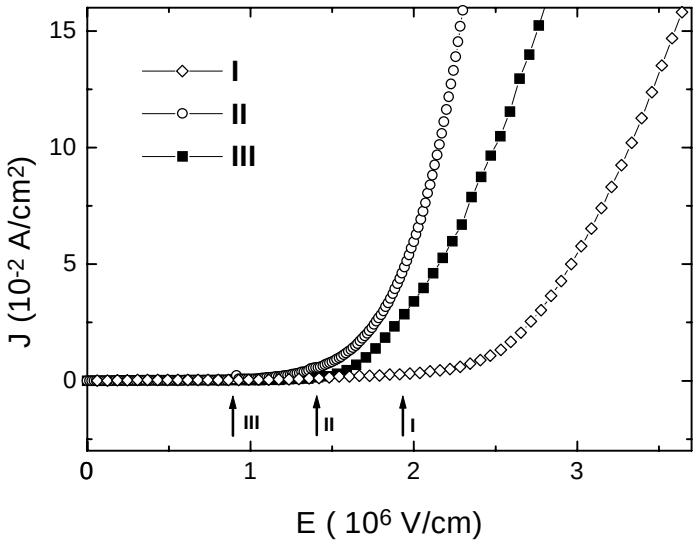

Figure 6.5 *Current density as a function of electric field for single layer ITO/Copolymer/Al devices. Arrows: the electric field strength at onset of emission.*

In figure 6.5 the I-V dependencies for all copolymer devices are plotted. The electric field strength at the onset of light emission for polymers **I** to **III** are equal to 1.9×10^8, 1.4×10^8 and 0.8×10^8 V/m, respectively. The consecutive lowering of the electric field is the result of the reduced HOMO-LUMO gaps, due to the substitution by octyloxy side-chains and cyano-groups onto the copolymer backbone, which decreases the barrier for electron injection.

Table 6.2 *Electrical properties and efficiencies of single-layer copolymer LEDs with ITO hole-injecting contacts in forward bias operation.*

Copolymer	Layer Thickness (nm)	Electrode	Bias voltage at turn-on (V)	Field at turn-on (10^8 V/m)	Ext.EL efficiency (10^{-2} ph/el)
I	80	Al	15	1.9	2.3
	80	Au	24	3.0	0.3
II	90	Al	13	1.4	0.9
III	140	Al	11.7	0.8	3.0

The hole-injection barrier

The injection of holes at the ITO anode into the polymer is controlled by a superposition of tunnelling and thermionic emission, the important parameter being the magnitude of the injection barrier [17,27]. At high fields, charge injection is dominated by tunnelling. The field dependence of the I-V characteristics were analysed using Fowler-Nordheim (FN) tunnelling theory in order to estimate the barrier heights for charge injection into the copolymer films. On the basis of this analysis we are able to roughly estimate the ionization potential or HOMO-level of the copolymers in an indirect way. In combination with the HOMO-LUMO gaps determined from the absorption spectra it is possible to derive an energy diagram for the copolymers. Fowler-Nordheim field emission tunnelling of electrons and holes through a triangular barrier gives [17,28]:

$$I \propto E^2 \exp\left(\frac{-\kappa}{E}\right) \quad , \tag{6.3}$$

$$\kappa = \frac{8\pi(2m^*)^{1/2}\varphi^{3/2}}{3qh} \tag{6.4}$$

where I is the current, E is the electric field, ϕ is the barrier height, m^* is the effective mass of the charge carriers (m^* is taken to be the free electron mass) and κ is a

parameter that depends on the barrier shape [29]. If Ln(I/E^2) versus $1/E$ is plotted, a linear dependence is obtained with a slope representing κ. In our ITO/copolymer/Al devices, the majority carriers are holes, due to the high work function of the electron injecting Al contacts. For this reason, they can be considered as "hole-only" devices. Therefore, FN analysis of the I-V curves in forward bias will yield the barrier heights between the hole-injecting ITO-contact and the molecular HOMO-level (Ionisation Potential, IP) of the copolymers. The FN analysis has been performed on at least three samples with different layer thickness, each consisting of four separate diodes. An example of a Fowler-Nordheim plot of a 95 nm thick ITO/Copolymer **I**/Al device is shown in figure 6.6.

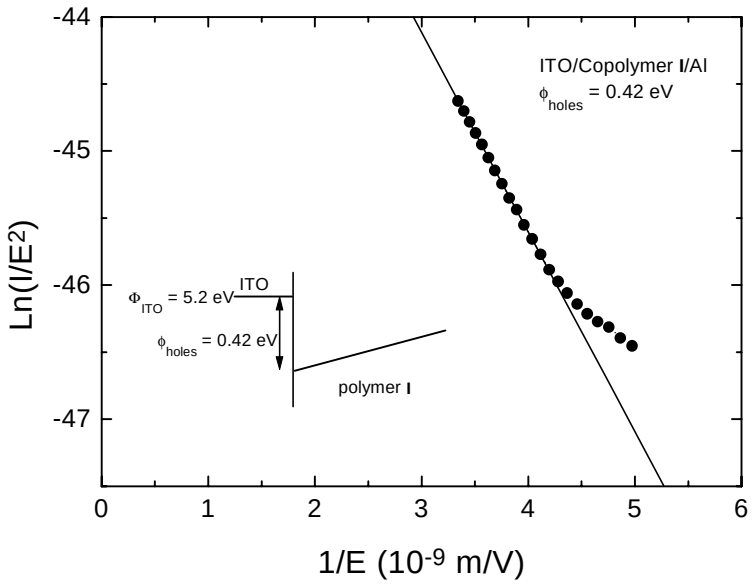

Figure 6.6 *Fowler-Nordheim plot for a 95 nm thick ITO/Copolymer **I** /Al device.*

The results of the FN-analysis of all four copolymers are summarized in table 6.3. The diode-to-diode and sample-to-sample reproducibility of the obtained barrier heights was reasonably good (±0.05 eV). Additionally, several devices were made with Au contacts to check the validity of the analysis for ITO/Al devices. The obtained barrier heights in ITO/Al and ITO/Au diodes were identical. This indicates that we indeed obtained the barrier for hole injection in ITO/Al diodes and that the contribution of the electron current to the total cell current can be neglected in such devices. The calculated hole injection barriers and ionization potentials (taking the work function of ITO to be ϕ_{ITO}= 5.2 eV) are listed in table 6.3. It should be explicitly stated that although the good reproducibility of the obtained barrier height, the absolute value for

the ionisation potential of the copolymers will be a rough estimate. This is caused by the influence of impurities, interface defects, bandbending, image force effects [29,30] , and the uncertainty in the value of the work function of ITO, which will lead to errors of the value of the barrier height and the ionization potential.

For this reason, cyclic voltammetry was used to determine the ionization potentials of the copolymers in solution as additional check to the Fowler-Nordheim analysis. With this electrochemical technique one can measure the oxidation potential of a molecule. The obtained oxidation potential can be converted to the ionization potential using an internal reference. Cyclovoltammograms were recorded in dichloromethane solution with tetrabutyl ammonium hexafluorophosphate as the electrolyte. The ferrocene/ferrocenium couple was used as internal reference to calibrate the cyclovoltammograms towards the Normal Hydrogen Electrode [16,31]. An ionization potential of 4.8 eV with respect to zero vacuum energy level was taken for ferrocene [32].

Table 6.3 *Ionization potentials and hole-injection barriers obtained by cyclic voltammetry and Fowler-Nordheim analysis.*

Copolymer	IP (eV) Cyclic voltammetry	ϕ_{holes} (eV) FN-analysis	IP (eV) FN-analysis
I	>5.8	0.4	5.6
II	5.7	0.2	5.4
III	5.8	0.3	5.5

The measured oxidation potentials were 0.9 and 1 Volts for the copolymers **II** and **III,** respectively. This corresponds to ionization potentials of 5.7 and 5.8 eV. The observed redox processes were reversible for both copolymers. For the copolymer **I,** no oxidation potential could be measured, due to oxidation of the electrolyte solution. This indicates that the oxidation potential of copolymer **I** is probably located beyond the measurement range. The trend in ionization potentials obtained with cyclic voltammetry corresponded with the trend obtained from Fowler-Nordheim analysis; only the absolute values are higher in the case of cyclic voltammetry.

In the copolymer LEDs the (hole) cell-current is determined by the injection barriers for holes in combination with the hole mobility in the copolymer. The trend in hole-injection barrier found for the copolymers corresponds with the observed electrical characteristics depicted in figure 6.5. The importance of the mobility for the cell current is reflected by the fact that the actual device current is usually several orders of magnitude smaller than the calculated Fowler-Nordheim tunnelling current. An explanation for this discrepancy was reported by Davids *et al.*[33]. They found that the low mobility in the polymer leads to a large backflow of injected carriers into the injecting contact, which decreases the injection rate of charges.

The copolymer diodes have external EL efficiencies of approximately $\approx 2\times10^{-2}$% ph/el, except for copolymer **II,** which has an efficiency of 9×10^{-3}% ph/el (see table 6.2). A rough estimate of the maximum external quantum efficiency achievable in an organic LED can be obtained from equation (6.5), which contains all factors governing the EL efficiency (Rothberg *et al.* [2]):

$$\Phi_{EL} = \chi \Phi_F \eta_R \eta_E \leq \left(\frac{1}{4}\right) \times 1 \times 1 \times \left(\frac{1}{2n^2}\right) \qquad (6.5)$$

where χ is the fraction of recombinations that result in a singlet exciton, Φ_F is the fraction of excitons that emit (PL quantum yield), η_R is the fraction of electrons and holes that recombine in the emissive layer and η_E the fraction of emitted photons that escape the emissive layer, which acts as a planar waveguide (*n* is the refractive index). According to a simple spin statistics argument of recombining e-h pairs (singlet:triplet generation rate is ≈1:3) , χ is limited to 0.25. The PL quantum efficiency Φ_F can be as high as unity. The fraction of e-h recombination η_R can also be close to unity if deep trapping is negligible and unipolar current flow is completely blocked. So the EL efficiency of an LED reflects the PL efficiency of the emissive layer. Based on equation (6.5) the upper limit of the external EL efficiency Φ_{EL} for copolymer **I**, for example, should be approximately 1.9 % (with n≈1.6 and $\Phi_F \approx 0.4$). The difference with the actual efficiency (2×10^{-2}%) illustrates the large imbalance of the electron and hole currents in our single-layer ITO/copolymer/Al diodes.

The trend found in EL efficiencies for our copolymers is in reasonable agreement with the trend in solid-state PL efficiencies (for PL efficiencies see table 6.1). However, if we compare copolymer **I** and **III,** we would expect a higher efficiency for copolymer **III**. From the energy diagrams depicted in figure 6.7, it is obvious that the electron and hole currents in a copolymer **III** device should be more balanced in comparison with copolymer **I**, and hence a larger value for η_R and a higher EL-efficiency would be anticipated.

Device optimization

From the preceding section it has become clear that the efficiency of single-layer devices is rather low due to unbalanced injection and transport of charge carriers. Electrons are not able to move far into the bulk due to trapping, resulting in an e-h recombination zone close to the metal electrode in a single-layer device, which has the effect of quenching the emission. Furthermore, the large unipolar loss current of holes, which do not recombine but are captured by the counter electrode, is significant in a single-layer device, reducing the efficiency greatly.

One way to optimize the efficiency of a device is by blending of the active material in a polymeric binder, which does not contribute to the emission. Bässler *et al.* [36] reported that blending of PPV in polystyrene (1:1 w/w) increased the efficiency approximately two orders of magnitude in comparison to a conventional PPV LED. Dilution of the polymer in a host matrix can have a two-fold effect. (1) An enhanced PL-efficiency due to the reduction of intermolecular exciton transfer to quenching sites, and (2) a reduction of the unipolar loss current (if the emitting polymer acts as a trap for holes).

Device optimization by means of electron transport molecules in a double-layer configuration has proven to be the most important approach to the enhancement of the quantum efficiency by well-balanced injection and transport [37,6]. The introduction of an electron-transport/hole-blocking layer (ETL) will move the recombination zone away from the interface. This is due to the introduction of an energy offset (hole-injection barrier) at the polymer/ETL interface, which prevents holes to cross the ETL layer, which results in a positive space-charge interfacial zone in the emissive layer. The space-charge zone will increase the field over the ETL layer, resulting in enhanced electron-injection from the cathode. Hence, e-h recombination takes place in a small region of the PPV layer near the heterojunction. The difference in EL efficiencies using Ca or Al as electron-injecting electrode in double-layer devices is smaller in comparison to single-layer devices. This is caused by the fact that the redistribution of the internal electric field by hole blocking has a larger effect on electron injection than the difference in the barrier height. A few examples of electron transport molecules are molecular acceptors with oxadiazole [37,38] and triazole [39,40] moieties. The most widely used transport molecule is 2-(4-*t*-butyl-phenyl)-5-(4-biphenyl)-1,3,4-oxadiazole (PBD). However, the main drawback of this molecule is its crystallinity. For this reason PBD is usually blended with an amorphous transparent host polymer, e.g. poly(methyl methacrylate) [38,6], to suppress crystallization. Loading of the host polymer is limited to 3:1 w/w PBD:PMMA. The disadvantage of this method is the reduced conductivity upon dilution resulting in higher operating voltages and device failure due to phase separation (recrystallization) of the blend under applied bias (device heating).

In our group, a novel PBD side-chain polymer (pPBD) was synthesized via a TEMPO-mediated "living" free-radical polymerization [41,42], which is used as electron transport layer in this study. The chemical structure is depicted in figure 6.8. The pPBD polymer has a molecular weight of M_w= 18,000 g.mol^{-1} (polydispersity 1.2), which corresponds to approximately 50 repeat units per chain. The polymer was soluble in toluene, and uniform layers could be prepared by spincoating. A rough estimate of the HOMO and LUMO levels for pPBD can be obtained by taking the values for vacuum-deposited PBD determined by photoemission and optical absorption measurements by Kido *et al.* [43]. PBD has its HOMO and LUMO at 5.9 and 2.4 eV. The HOMO-LUMO gap of pPBD determined by the onset of absorption

(see figure 6.8) was approximately 3.4 eV, which is close to the HOMO-LUMO gap value found by Kido for PBD.

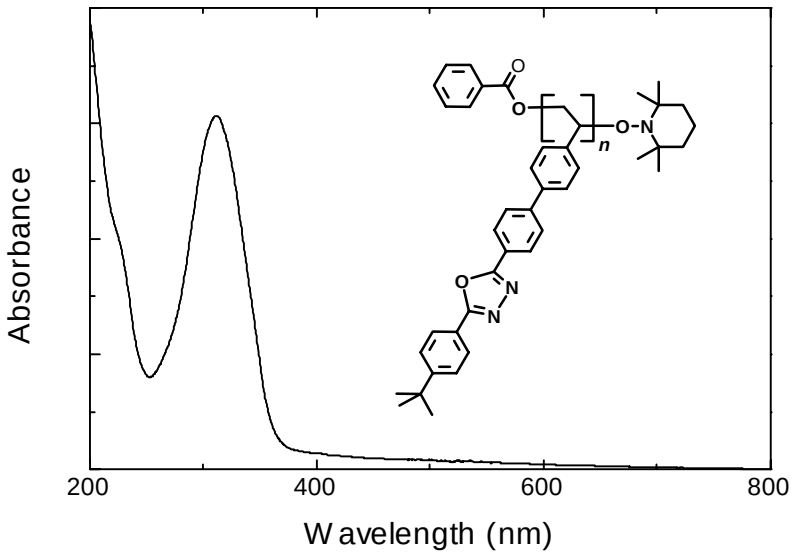

Figure 6.8 *Chemical structure and absorption spectrum (film) of pPBD.*

Double-layer devices were prepared with copolymer **III** as emissive layer. The total layer thickness of the devices was ≈110 nm. It was impossible to determine the thickness of the individual layers in an accurate way, due to the good solubility of the two polymers, which will make the pPBD solution wash a fraction of the initial copolymer **III** away. Spincoating of the pPBD polymer on glass with the same rotation speed used for the preparation of the heterojunction gave a layer thickness of 40 nm. The maximum external efficiency measured in the double-layer devices was approximately 0.12 % ph/el, with a maximum brightness of approximately 250 cd/m^2. However, the reproducibility between different diodes and samples was poor.

In addition, blends of copolymer **III** and pPBD were made. Single-layer devices consisting of blends with 38 w% and 63 w% pPBD were prepared. Based on the HOMO and LUMO-levels of both compounds, copolymer **III** should act as a trap for both electrons and holes. Furthermore, it is expected that the loss current of the majority carriers will decrease and that exciton diffusion to quenching sites is further diminished due to dilution. Indeed the efficiency increased to 0.04 and 0.08 % (at low drive-current) for the blend with 38 w% and 63 w% pPBD, respectively, but the I-V-curves shifted to higher fields with increasing content of pPBD (see figure 6.9). This

is the result of the higher barrier for injection in pPBD, which limits the injection of both holes and electrons. The maximum luminance reached is highest for the blend with 38 w% pPBD, because the blend with 63 w % pPBD sustains lower current before device breakdown occurred. The PL and EL spectra were blue-shifted (yellow emission) compared to that of pure copolymer **III** due to dilution in pPBD, indicating that copolymer **III** is molecularly dispersed in pPBD. So blending increased the efficiency to 0.08 %, but has as drawback that higher operating voltages have to be applied.

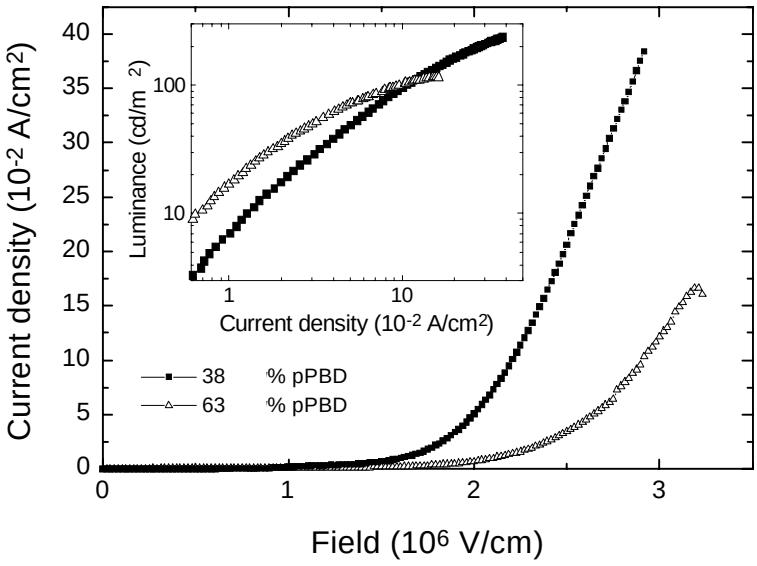

Figure 6.9 *I-V characteristics of single-layer LEDs containing blends of copolymer **III** with pPBD (38 and 63 w%). Inset: luminance as a function of drive current.*

The most efficient polymer LEDs up to date are based on double-layer devices made from PPV and cyano-substituted PPV derivatives. Internal efficiencies up to 4% are reported for such heterojunction polymer LEDs [7,44]. The cyano-substituted PPV derivatives are highly fluorescent and the strong electron-accepting cyano groups on the vinylene linkages lower the LUMO-level (and HOMO-level to a lesser extent) of the polymer, which makes them useful as both electron transport and emissive layer. The offset in HOMO and LUMO level at the polymer/polymer interface will block both holes and electrons, resulting in balanced transport, which is schematically depicted in figure 6.10.

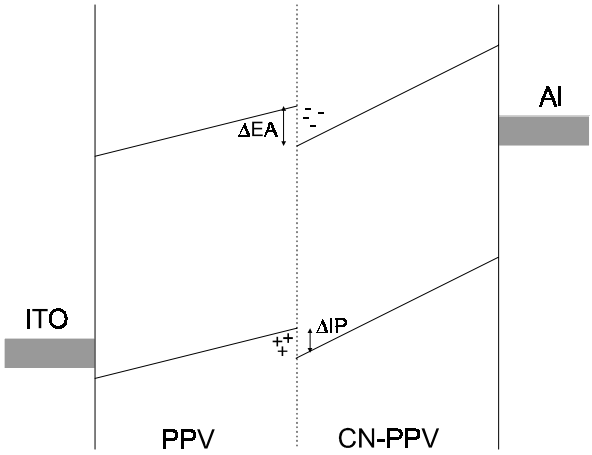

Figure 6.10 *Schematic energy level diagram for a two-layer LED under forward bias (from reference [7]).*

By confining the charges in the interface region, a large field is built up, which promotes tunnelling through the heterojunction. Emission is established when a hole tunnels through the barrier and recombines in the CN-PPV layer or when an electron tunnels through the barrier and forms an exciton in the PPV layer, which then migrates into the lower-energy CN-PPV polymer and radiatively decays. Thus, emission is almost solely produced in the CN-PPV layer.

We applied this concept to obtain enhanced device efficiencies for the cyano-substituted copolymer **III**. Double-layer devices were prepared by spin-casting copolymer **II** from a chloroform solution onto ITO substrates. After drying of the layer under vacuum, copolymer **III** was spin-cast on top of the copolymer **II** layer and Al-electrodes were deposited as electron-injecting contacts. The highest measured external efficiency obtained from a 190 nm thick double-layer device was 7×10^{-2}% ph/el, which is twice as high in comparison with the single layer copolymer **III** devices. The EL-emission spectrum corresponded with the PL spectrum of copolymer **III**, as expected. The diode-to-diode (on the same device) and device-to-device reproducibility of the double-layer devices was poor. This is mainly caused by the good solubility of both copolymers in the solvents used for processing, as mentioned in the preceding section. A large part of the copolymer **II** layer was washed away upon casting of copolymer **III** and substantial mixing of the two copolymers resulted in an ill-defined interface. We were unable to determine the individual layer thickness of the two copolymers in the devices in an accurate way. The efficiency enhancement was rather poor in comparison with that reported in literature. The most plausible reasons for the poor enhancement are the ill-defined interface region and the fact that

the offset between the HOMO-levels of the two polymers, ≈ 0.1 eV, was most probably too small to achieve significant hole blocking.

A second set of devices was made with a hole-transport layer of PPV prepared via the so-called sulphonium precursor route [45]. This polymer has a molecular weight of $M_w \approx 1\times10^6$ g.mol^{-1} as determined by GPC. The precursor was spincast from methanol solution onto the ITO substrates and thermally converted to PPV at 220 ^{O}C for 6 hours. The thickness of the PPV layer was approximately 50 nm as determined with a profilometer. The major advantage of this polymer is that it is fully insoluble after conversion, which assures the formation of a well-defined heterojunction. A 70 nm thick layer of copolymer **III** was spin-coated on top. In this case external efficiencies up to 0.4 %ph/el and brightnesses up to approximately 600 cd/m^2 were achieved, which is substantially higher than in the previous case. These values correspond to an internal efficiency of ≈2 %, approaching the maximum achievable efficiency of 10 % based on theoretical considerations. The exact ionization potential (IP) and electron affinity (EA) values of PPV are unknown. Values for IP and EA of 5.05 and 2.32 eV, based on quantum chemical calculations by Brédas [46], would imply to barriers of roughly 0.3–0.4 eV for both holes and electrons at the heterojunction.

6.3.2 Oligo(*p*-phenylene vinylene)s

A series of three different five-ring oligo(*p*-phenylene vinylene)s (OPVs) has been studied as active layer in Light-Emitting Diodes. The chemical structures of the OPVs employed for this study are depicted in figure 6.11. The synthesis and characterization of the model compounds can be found in reference [47] and the optical properties in chapter 2 of this thesis. In first instance, non-optimized single-layer LEDs were prepared by vacuum sublimation following the procedure described in the experimental section. All thin layers of the different OPVs showed similar morphologies in the optical microscope after deposition onto the ITO substrates. The electrical properties and efficiencies for the series of ITO/OPV/Al and Ca (for Ooct-OPV5) single-layer devices are summarized in table 6.4. From all OPVs working LEDs could be prepared. It should be stated that the minimum thickness of the active layer must be of the order of 150 nm and thicker to obtain reproducible diode characteristics. Thinner devices all suffered from shorts and non-uniform light emission over the active area of the diodes. In figure 6.12 the current-voltage characteristics are shown for all OPVs in a single-layer configuration with electron-injecting Al contacts. The arrows indicate the electric field strength at which light emission was detectable. All ITO/OPV/Al diodes showed rectifying behaviour and we were not able to observe electroluminescence in reverse bias for any of the OPV-based devices.

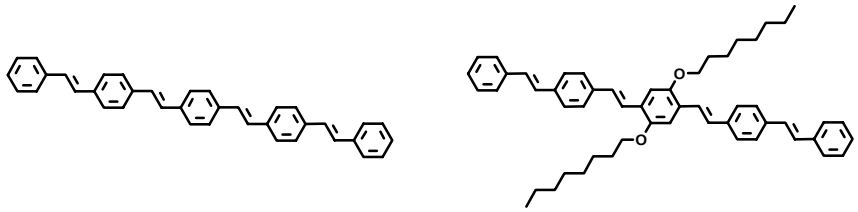

OPV5 **Ooct-OPV5**

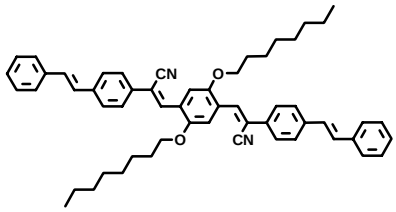

Ooct-OPV5-CN2

Figure 6.11 *Chemical structure of the oligo(p-phenylene vinylene)s.*

Table 6.4 *Electrical properties and efficiencies of the single-layer and double-layer oligomer LEDs with ITO hole-injecting contacts in forward bias operation.*

Oligomer[a]		Cathode	Layer thickness (nm)	$V_{turn-on}$[b] (V)	$E_{turn-on}$ (10^8 V/m)	Ext. eff. (10^{-2} %)
OPV5	As	Al	380	18.1	0.5	1.1
Ooct-OPV5	As	Al	193	24.4	1.3	0.1
	An			20.4	1.1	1.2
	As	Ca	183	11.8	0.6	10.0
Ooct-OPV5-CN2	As	Al	150	20	1.3	1.5
Ooct-OPV5/ Ooct-OPV5-CN2	As	Al	150/45	8.7	0.5	31

a) As: as-deposited, An: annealed. b) turn-on is defined here as the point at which the emission is detectable.

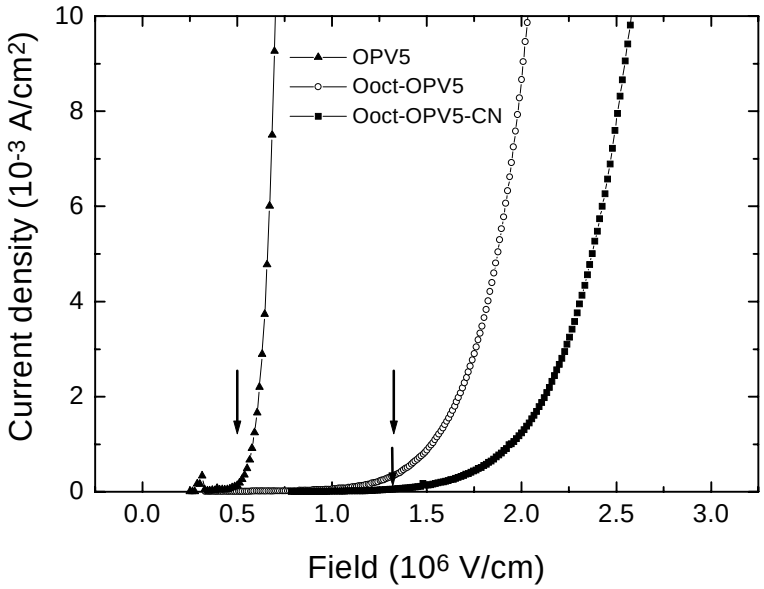

Figure 6.12 *Electrical characteristics (current density versus electric field) of the ITO/OPV/Al devices. The arrows indicate the onset of light emission.*

Electrical measurements on devices with different layer thickness showed that the diode current depends on the applied field rather than the drive voltage. The same behaviour as was observed with the alternating PPV copolymers. This indicates that field-driven injection determines the electrical characteristics. From figure 6.12 it is evident that OPV5 has the lowest onset for both current and emission. By means of Fowler-Nordheim analysis of the I-V characteristics and optical absorption measurements we estimated the injection barrier for holes and the HOMO-LUMO bandgap, respectively. The results of this analysis are given in table 6.5. The difference between the onset of current and light, for OPV5 and Ooct-OPV5, is significant and contradicts to the band offsets derived from table 6.5:

(a) The onset for light emission for OPV5 appears at half the electric field strength of Ooct-OPV5, while the barrier for electron-injection is approximately 0.3 eV higher.

(b) The IV-characteristics are determined by the majority carriers in these devices, which are holes. On the basis of the similar hole-injection barrier for both OPVs, one would expect approximately the same electrical characteristics.

A possible explanation for this discrepancy could be that the charge-carrier mobilities (holes and electrons) in the case of OPV5 are much higher, resulting in a higher injection rate of charge carriers [33]. If we now compare the electrical characteristics of Ooct-OPV5 and Ooct-OPV5-CN2 it is obvious that the onset of current appears at higher drive field in the case of Ooct-OPV5-CN2. This is consistent with the value found for the hole-injection barrier, which is 0.2 eV higher. However, the onset of emission appears at the same field as for Ooct-OPV5, which reflects the lowering of the LUMO-level due to the presence of cyanogroups (approximately 0.5 eV lower than that of Ooct-OPV5). The external EL efficiencies of the single-layer OPV devices were typically in the range of 0.01–0.02 %ph/el. Only the EL efficiency of the Ooct-OPV5 devices was an order of magnitude lower. On the basis of the PL efficiencies, which were all in the same range (40-50 %), one would expect similar values for Ooct-OPV5.

Table 6.5 *Estimated HOMO-LUMO gaps and hole-injection barriers.*

Oligomer	HOMO-LUMO gap (eV)[a]	ϕ_{holes} (eV)[b]
OPV5	2.7	0.2
Ooct-OPV5	2.4	0.2
Ooct-OPV5-CN2	2.1	0.4

a) Optical absorption measurements b) Fowler-Nordheim analysis

To optimize the performance of single-layer Ooct-OPV5 devices, Ca instead of Al was used as cathode, which lowers the injection barrier for electrons with approximately 1.3 eV. The change of cathode resulted in a more than twofold reduction of the drive field at turn-on (6×10^7 V/m) and two orders of magnitude enhancement in EL efficiency (0.1 %), due to improved electron-injection.

The electroluminescence spectra of the single-layer devices are depicted in figure 6.13. All EL spectra coincided with the solid-state photoluminescence spectra, indicating that the same excited states are involved in both PL and EL. The broad luminescence spectrum for Ooct-OPV5-CN2 is attributed to excimer emission (see chapter 2).

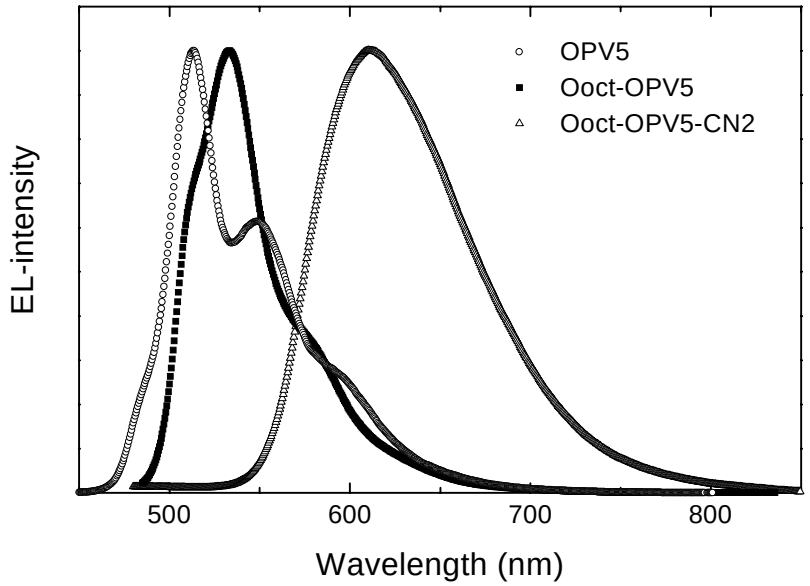

Figure 6.13 *Electroluminescence spectra of the ITO/OPV/Al devices.*

The influence of morphology on the device performance

The influence of the thin-film morphology on the device performance was investigated for Ooct-OPV5 by means of annealing (as described in chapter 2 and 5). For Ooct-OPV5 annealing leads to an increase of the single-crystal domain size and an enhanced molecular orientation (see chapter 2). The external efficiency of the annealed Ooct-OPV5 films was more than one order of magnitude higher than that of the as-deposited film (inset figure 6.14). The photoluminescence quantum yield as measured under laser illumination in an integrating sphere was approximately 20 % larger for the annealed film. If we assume that photoexcitation and charge injection give rise to the same excited state (the singlet exciton), the 20 % rise in PL efficiency alone, cannot account for the 10-15 fold increase in EL efficiency. As can be seen from figure 6.14 there is no significant difference in cell current upon annealing. The majority charge carriers in these devices are holes, so we may infer that the hole current is the same for both morphologies. Fowler-Nordheim analysis of the IV-characteristics revealed that the barrier for hole-injection is the same for both morphologies, and from the similar absorbance spectra of both morphologies we can conclude that the bandgap doesn't change upon annealing.

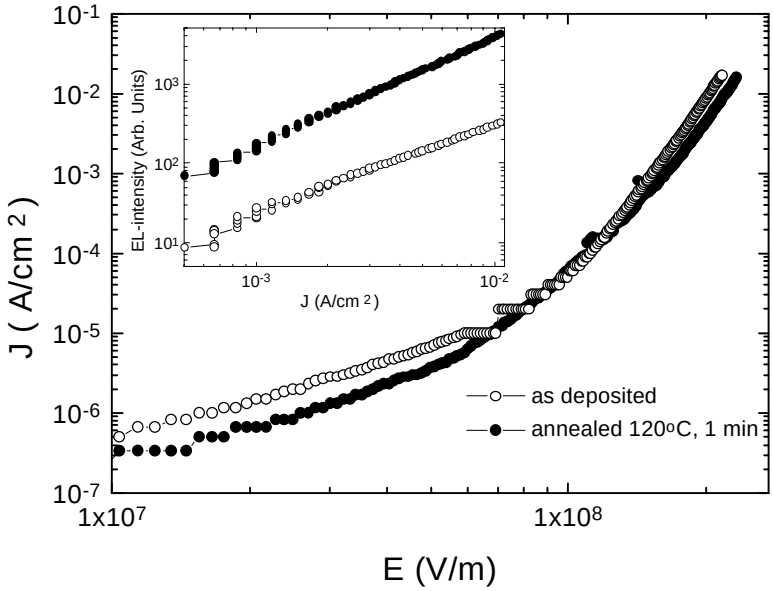

Figure 6.14 *J-E characteristics for a single-layer ITO/Ooct-OPV5/Al devices with an as-deposited and an annealed active layer, respectively. Inset: Luminance as a function of cell current for both thin-film morphologies.*

The electron current in such devices is much smaller and is fully masked by the current of the majority carriers. For this reason Al/Ooct-OPV5/Ca devices were prepared, which can be considered as "electron-only" devices. In the annealed "electron-only" devices the current was approximately one order of magnitude higher. Hence, it seems that the increase in efficiency upon annealing can be attributed to an increase of electron mobility. The improvement of molecular orientation and the reduction of the density of grain boundaries upon annealing may be considered as possible explanations for the improved electron mobility. For Ooct-OPV-CN2 and OPV5 it was not possible to prepare working devices with annealed layers. Annealing resulted in the formation of small holes in the evaporated films causing short-circuited devices.

Double-layer devices

Double-layer devices were prepared, consisting of an Ooct-OPV5 hole-transport layer and an Ooct-OPV5-CN2 electron-transport/emissive layer to balance charge transport and injection. The device characteristics are summarized in table 6.4 and depicted in figure 6.15. The voltage at which EL was detectable was also significantly reduced to

8.7 Volts (4.5×10^7 V/m). External efficiencies up to 0.31 % were reached in an ITO/Ooct-OPV5(150 nm)/Ooct-OPV5-CN2(45 nm)/Al device, which corresponds to an internal efficiency of ≈1.5 %. A more than one order of magnitude enhancement of the efficiency in comparison to single-layer Ooct-OPV5-CN2 devices. Despite the high EL efficiency, only low current levels were reached before critical device failure, which resulted in a maximum brightness of only ≈30 cd/m^2. Orange/red emission was observed above turn-on in the double-layer device indicating that Ooct-OPV5-CN2 is the emissive species in the device. However, the electroluminescence spectrum (inset figure 6.15) revealed that there is a small contribution of EL emission originating from Ooct-OPV5 (see arrow in the inset).

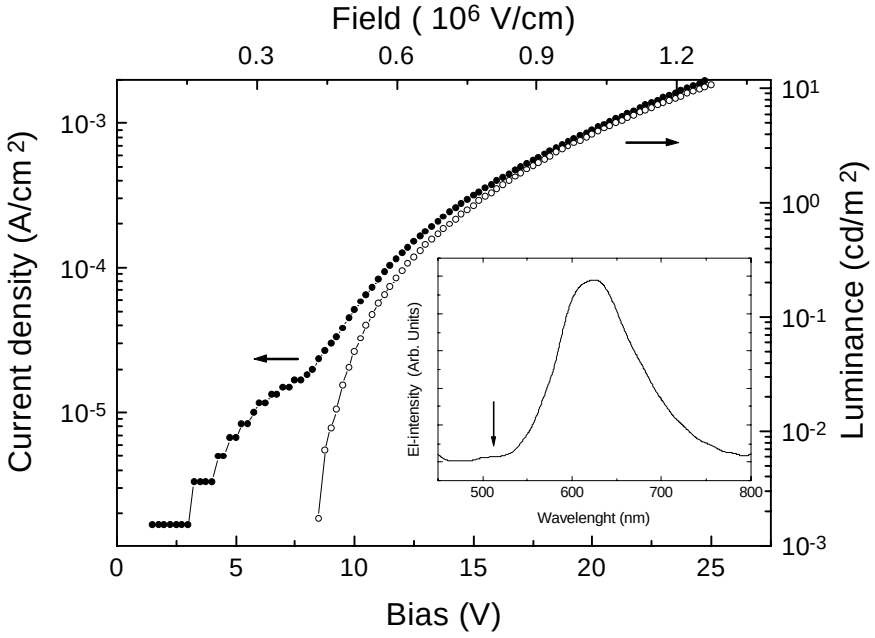

Figure 6.15 *Semilog plot of current density (closed circles) and luminance (open circles) of an ITO/Ooct-OPV5(150 nm)/Ooct-OPV5-CN2(45 nm)/Al double-layer device as a function of bias voltage. Inset: double-layer electroluminescence spectrum.*

6.4 Conclusions

Electroluminescence was achieved in the blue, green and orange wavelength region with single-layer devices consisting of transparent indium-tin-oxide anodes and air-stable Al cathodes. The efficiencies of the single-layer copolymer/oligomer LEDs are comparable to those reported for fully conjugated PPVs. Fowler-Nordheim tunnelling theory was used to analyse the current-voltage characteristics in order to determine the barriers for hole injection in the single-layer devices. In combination with cyclic

voltammetry and optical absorption measurements it was possible to estimate energy diagrams for all copolymers and oligomers, which could be used to describe the results obtained in a qualitative way. Furthermore, the influence of the thin-film morphology on LED performance has been investigated for the octyloxy-substituted oligo(*p*-phenylene vinylene). The EL efficiency is drastically increased for Ooct-OPV5 films with improved molecular orientation and larger crystalline domains sizes, which is attributed to enhanced electron transport.

Device optimization by means of additional charge-transport layers to enhance the electroluminescence efficiency has been applied successfully. Balanced hole and electron currents, and e-h recombination distant from the metal cathode are probably achieved in such devices, resulting in improved device performance. A novel polymer with oxadiazole-based side-chains has been used successfully as an electron-transport/hole-blocking layer. In combination with a cyano-substituted PPV copolymer as the emissive layer, external EL efficiencies up to 0.1 % were obtained. The best-performing double-layer LEDs were based on the electronegative cyano-substituted copolymers and oligomers as the electron-transport/emissive layer. In this case, external electroluminescence efficiencies up to 0.3-0.4 % are reached.

6.5 References

[1] J.H. Burroughes, D.D.C. Bradley, A.R. Brown, R.N. Marks, K. Mackay, R.H. Friend, P.L. Burns and A.B. Holmes, *Nature*, **347**, 537 (1990)
[2] L.J. Rothberg, A.J. Lovinger, *J. Mater. Res.*, **11**, 3174 (1996)
[3] R. H. Friend, G.J. Denton, J.J.M. Halls, N.T. Harrison, A.B. Holmes, A. Köhler, A. Lux, S.C. Morratti, K. Pichler, N. Tessler, K. Towns, H.F. Wittmann, *Solid State Commun.*, **102**, 249 (1997)
[4] D. Braun and A.J. Heeger, *Appl. Phys. Lett.*, **58**, 1982 (1991)
[5] C. Zhang, H. von Seggern, K. Pakbaz, B. Kraabel, H.-W. Schmidt, A.J. Heeger, *Synth. Met.*, **62**, 35 (1994); J.K. Herrema, J. Wildeman, R.H. Wieringa, R.E. Gill, G.G. Malliaras, S.S. Lampoura, G. Hadziioannou, *Polym. Preprints*, **34**, 282 (1993)
[6] D.D.C. Bradley, *Synth. Met.*, **54**, 401 (1993)
[7] N.C. Greenham, S.C. Moratti, D.D.C. Bradley, R.H. Friend and A.B. Holmes, *Nature*, **365**, 628 (1993)
[8] C. Zhang, D. Braun, A.J. Heeger, *J. Appl. Phys.*, **73**, 5177 (1993)

[13] M.D. Joswick, I.H. Campbell, N.N. Barashkov, J.P. Ferraris, *J. Appl. Phys.*, **80**, 883 (1996); T. Goodson III, L. Wenjie, A. Gharavi, L. Yu, *Adv. Mater.*, **9**, 639 (1997)
[14] J. Servet, G. Horowitz, S. Ries, O. Lagorsse, P. Alnot, A. Yassar, F. Deloffre, R. Srivastava, R. Hajlaoui, P. Lang, F. Garnier, *Chem. Mater.*, **6**, 1809 (1994)
[15] G.A. Mabbot, *J. Chem. Ed.*, **60**, 697 (1983)
[16] R.R. Gagné, C.A. Koval, G.C. Lisensky, *Inorg. Chem.*, **56**, 462 (1984)
[17] I.D. Parker, *J. Appl. Phys.*, **75**, 1656 (1994)
[18] D.V. Morgan, Y. Aliyu, R.W. Bunce, *Phys. Status Solidi A*, **133**, 77 (1992)
[19] I.H. Campbell, T.W. Hagler, D.L. Smith, J.P. Ferraris, *Phys. Rev. Lett.*, **76**, 1900 (1996)
[20] Handbook of Chemistry and Physics (CRC press, Boca Raton, Florida, 1986)
[21] A. Hilberer, P.F. van Hutten, J. Wildeman, G. Hadziioannou, *Macromol. Chem. Phys.*, **198**, 2211 (1997)
[22] M.P.L. Werts, Synthesis of cyano-substituted PPV-polymers for LEDs (undergraduate report, University of Groningen, 1996)
[23] J.L. Brédas, *Adv. Mater.*, **7**, 264 (1995)
[24] J. Grüner, R.H. Friend, J. Huber, U. Scherf, *Chem. Phys. Lett.*, **251**, 204 (1996)
[25] H. Antoniadis, M.A. Abkowitz, B.R. Hsieh, *Appl. Phys. Lett.*, **65**, 2030 (1994)
[26] D. Braun, A.J. Heeger, *Appl. Phys. Lett.*, **58**, 1982 (1991)
[27] S. Karg, W. Riess, V. Dyakonov, M. Schwoerer, *Synth. Met.*, **54**, 427 (1993)
[28] R.H. Fowler, L. Nordheim, *Proc. R. Soc., London Ser. A.*, **119**, 173 (1928)
[29] M. Lampert, Current injection in solids (Academic Press, New York, 1970), 189
[30] Y. Yang, Q. Pei, A.J. Heeger, *J. Appl. Phys.*, **79**, 934 (1996)
[31] G. Gritzmer, J. Kuta, *Pure Appl. Chem.*, **56**, 462 (1984)
[32] H.M. Koepp, H. Wendt, H. Strehlow, *Z. Electro Chem.*, **64**, 483 (1960)
[33] P.S. Davids, Sh.M. Kogan, I.D. Parker, D.L. Smith, *Appl. Phys. Lett.*, **69**, 2270 (1996)
[34] K.N. Backer, A.V. Vratini, T. Resch, H.C. Knachel, W.W. Adams, E.P.Socci, B.L. Farmer, *Polymer*, **34**, 1571 (1993)
[35] B. Champagne, D.H. Mosley, J.G. Fripiat, J.-M. André, *Phys. Rev. B*, **54**, 2381 (1996)
[36] H. Vestweber, J. Oberski, A. Greiner, W. Heitz, R.F. Mahrt, H. Bässler, *Adv. Mat. Optics Elect.*, **2**, 197 (1993)
[37] C. Adachi, T. Tsutsui, S. Saito, *Appl. Phys. Lett.*, **57**, 531 (1990)
[38] A.R. Brown, D.D.C. Bradley, P.L. Burns, J.H. Burroughes, R.H. Friend, N.C. Greenham, A.B. Holmes, A. Kraft, *Appl. Phys. Lett.*, **61**, 2793 (1992)
[39] J. Kido, C. Ohtaki, K. Hongawa, K. Okuyama, K. Nagai, *Jpn. J. Appl. Phys.*, **32**, L917 (1993)
[40] M. Strukelj, F. Papadimitrakopoulos, T.M. Miller, L.J. Rothberg, *Science*, **267**, 1969 (1995).
[41] M. Moroni, A. Hilberer, G. Hadziioannou, *Macromol. Rapid. Commun.*, **17**, 693 (1996)
[42] M. Moroni, A. Hilberer, G. Hadziioannou, *Macromolecules* (1997) submitted
[43] J. Kido, *Appl. Phys. Lett.*, **67**, 2281 (1995)
[44] D.R. Baigent, N.C. Greenham, J. Grüner, R.N. Marks, R.H. Friend, S.C. Moratti, A.B. Holmes, *Synth. Met.*, **67**, 3 (1994)

[45] A. Delmotte, M. Biesman, H. Rahier, M. Gielen, E.W. Meyer, *Synth. Met.*, **58**, 325 (1993)
[46] J.L. Brédas, *Adv. Mater.*, **7**, 263 (1995)
[47] R.E. Gill, Design, synthesis and characterization of luminescent organic semiconductors (Ph.D. thesis, University of Groningen, 1996), chapter 3